

Original Article: Silver Nanoparticles Decorated Functionalized Multiwalled Carbon Nanotubes Modified Screen Printed Sensor for Voltammetric Determination of Butorphanol



Manish S. Sengara^a | Sachin Saxena^{a,*} | Soami P. Satsangee^a | Rajeev Jain^b

^a USIC, Dayalbagh Educational Institute, Dayalbagh, Agra-282005, India

^b Pondicherry University, Puducherry-605014, India



Citation M. S. Sengar, S. Saxena*, S. P. Satsangee, R. Jain, **Silver Nanoparticles Decorated Functionalized Multiwalled Carbon Nanotubes Modified Screen Printed Sensor for Voltammetric Determination of Butorphanol.** *J. Appl. Organomet. Chem.*, 2021, 1(2), 95-108.

<https://doi.org/10.22034/jaoc.2021.289344.1023>



Article info:

Received: 5 May 2021

Accepted: 10 Jun 2021

Available Online: 22 Jun 2021

ID: JAOC-2106-1023

Checked for Plagiarism: Yes

Peer Reviewers Approved by:

Dr. SUNIL V. GAIKWAD

Editor who Approved Publication:

Professor Dr. Abdelkader Zarrouk

Language Editor

Dr. Behrouz Jamalvandi

Keywords:

Butorphanol, Ag/CNT/SPE, Sensor, Voltammetry.

ABSTRACT

The present study aimed at describing silver nanoparticles based functionalized multiwalled carbon nanotubes modified screen printed carbon electrode (Ag/CNT/SPE) for an effective determination of an opioid analgesic drug butorphanol (BTR). The suspension of Ag/CNT prepared was drop casted onto the surface of SPE. The surface morphology of the nanocomposite was studied using XRD, FESEM, EDX, FT-IR, and UV-Vis. Ag/CNT/SPE showed a remarkable enhancement in the peak current values in cyclic and square wave voltammograms when compared with that of the CNT/SPE, Ag/SPE and bare carbon SPE. The anodic phenomenon of BTR occurring at Ag/CNTs/SPE was found to be a function of pH of the medium, concentration and scan rate of BTR. The oxidation peak current was found proportional to the BTR concentration within the linear range of 1.05-10.45 μM , with a detection limit of 2.15 μM (LOD) and the quantification limit of 7.18 μM (LOQ). The redox mechanism of BTR at the modified electrode was evaluated after optimizing the electrode dynamic parameters. The sensor was further scrutinized for the successful quantification of BTR in the pharmaceutical formulation.

Introduction

Chemical and pharmaceutical pollution mixes with soil, water and air, posing serious health and environmental problems to the world. Remediation and detection of such substances therefore becomes essential with simple, cost

effective and ultra-trace determination technology. These features are provided by the synergism of electrochemical methods and nanotechnology [1]. Electrochemical method which is a subdivision of analytical chemistry provides information related to amounts, properties and environments of chemical species; it involves low cost manufacturing

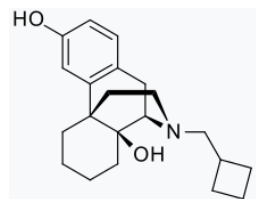
*Corresponding Author: Sachin Saxena (sachinusic@gmail.com)

processes. Nowadays, screen printed electrodes (SPE) have prominent use in analytical chemistry, where few drops of sample solution is needed on the SPE to detect analyte system with high sensitivity and selectivity, thereby reaching technologically to miniaturization, with possible use in clinical [2], environmental [3], and pharmaceutical [4], analysis. Working analytical behavior of SPE can further be improved with synergism of nanoparticles [5, 6], conducting polymer [7] and carbon-based materials [8] due to large surface area, stability and conductivity [9]. Graphene, graphene oxide, fullerenes, and carbon nanotubes (CNTs) can be deposited onto screen printed sensors by different methodologies including with drop casting, electro-deposition and inkjet printing [10, 11]. Detection of pharmaceuticals with electrochemical method is very rapid, simple and cost-effective technique. Further, this analytical technique is a good alternative compared with other analytical techniques with the ability to detect highly selective and sensitive ultra- trace analytes in the solution system [12, 13].

CNTs have been exploited in different fields owing to their excellent properties for e.g. high mechanical strength, strong adsorption ability and high conductivity. When it was mixed with metal, metal oxide then these properties of CNTs is enhanced due to increase in surface area, electron transfer and in electrical and mechanical strength [14]. Main advantage of using CNTs is their small size, applicability for macro-assemblies and ultimate fibril structure. Metallic nanoparticles are used with CNTs due to their size dependent properties. These properties attract the attention of researchers during last decades. Thus, in this study silver nanoparticles were used with CNTs. It enhances the antibacterial, electrical and thermal properties in an excellent manner. It is also used as a contact material in electrical circuits; therefore, prepared composites have better electron transfer rate [15, 16]. CNTs have been reported as the most appealing materials to support silver nanoparticles to form efficient disinfectant. CNTs dispersion in the matrix is the major problem; therefore, CNTs are functionalized by

different ways, e.g., acid treatment and amination process. During functionalization of CNTs, functional group like -NH_2 , -OH and -COOH get bonded onto the surface, which support silver nanoparticles to anchor on CNTs. Thus, Ag/CNT composite has a better electron transfer and excellent sensitivity [17].

Butorphanol (BTR, Scheme 1) is a synthetic agonist-antagonist opioid analgesic drug, most closely structurally related to Morphine, Codeine and Levorphanol. BTR is widely used as a drug for the veterinary scientists to study effects of the drug on the dogs, cats, birds etc. The drug chemically denoted as (1S,9R,10S)-17-(cyclobutylmethyl)-17-azatetracyclo[7.5.3.0^{1,10}.0^{2,7}] heptadeca-2(7),3,5-triene-4,10-diol);2,3-dihydroxybutanedioic acid is frequently prescribed for the accidental pain in small mammals. Different techniques have been explored for the determination of BTR both in the bulk form, pharmaceutical formulation and in the biological fluids such as blood plasma, blood serum, urine samples and even in the environmental samples, which include HPLC [18], luminescence [19], liquid chromatography-mass spectrometry [20], gas chromatography-mass spectrometry [21] and capillary isotachophoretic [22]. However, these techniques involve costlier sophisticated equipments with time taking complexity of preparation of real samples before introducing it to the system for analysis [23].



Scheme 1. Butorphanol

Niwa research on a theme named effects of BTR and its metabolites on the levels of monoamines in the Rat Brain, described the fate of BTR and its main mechanism. It was found that the Norbutorphanol and hydroxybutorphanol were the present in several parts of rat brain which was then compared with pentazocine and morphine utilizing the HPLC-ECO method [24].

Troncyet *al.* (1996) studied pharmacokinetics of epidural BTR in isoflurane-anaesthetized dogs. They reported recovery of BTR from Dog's blood, from eight of the dogs they received 0.25 mg/kg and the maximum concentration were obtained 42.28 ng/mL at 13.88 min in blood, and 18.03 ng/mL at 30 min in CSF. Volume of distribution, clearance, mean distribution and elimination half-lives were respectively 4.39 L/kg, 2.02 L/h.kg. 16.5 min and 189.1 min [25].

The present work offers a favourable and schematic electrochemical approach towards the fabrication of Ag/CNT/SPE, which was investigated for the analysis of electrochemical behavior of BTR under the optimized conditions using cyclic voltammetry (CV) and squarewave voltammetry (SWV). Ag nanoparticles dispersion with functionalized CNT matrix has been elucidated by the structural and morphological analysis of the nanocomposite using various surface characterizations and spectroscopy techniques. Ag/CNT/SPE showed a remarkable enhancement in the current response of the oxidation process of BTR in comparison to the bare SPE.

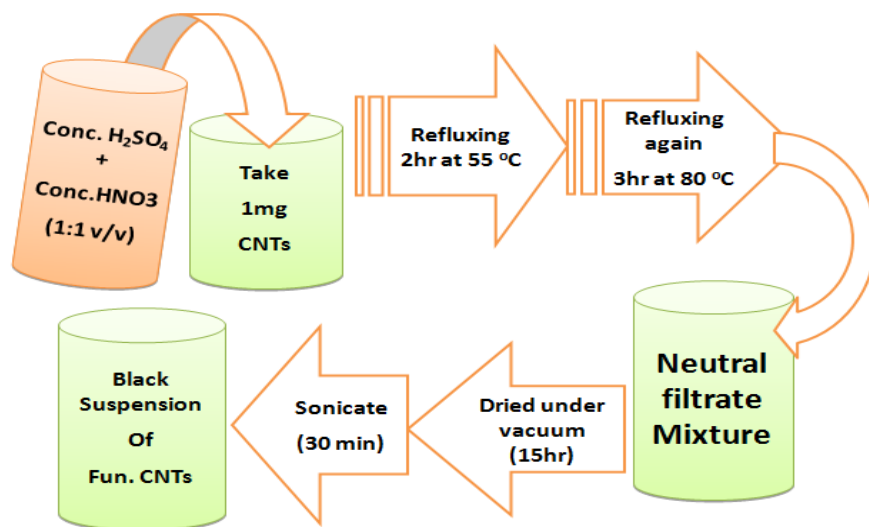
Experimental

Apparatus and materials

Voltammetric measurement (CV, SWV) were performed on DROPSENS μ STAT 400. Screen Printed Electrode (SPE-110) used for the study were directly purchased from Metrohm. SPE consisted of three electrode patterns printed on the sheet with the help of carbon and Ag inks. All reagents and solvents employed in present research work were of analytical grade. The solutions were made in Milli-Q water (resistivity 18 M Ω -cm) generated from Elga water purification system. Silver nitrate was purchased from Merck. Millipure (purity > 99%), SPE and CNTs were obtained from metrohm while DMF, ascorbic acid, orthophosphoric acid and NaOH were purchased from Fisher scientific (India).

Acid functionalization of CNTs

CNTs were functionalized by refluxing with conc. H₂SO₄ and HNO₃ (1:1 v/v) at 55 °C and 80°C for removal of unreacting impurities from the suspension, filtrate became neutral followed by drying in vacuum for 15 hr and sonicated till black suspension was formed. This functionalization process is a type of acid oxidation of CNTs which acquires hydroxyl and carboxylic functional groups as shown in Scheme 2. [27].



Scheme 2. Flowchart representation for Acid Functionalization of CNTs

Electrochemical methods

Ag nanoparticles have been prepared using green route process utilizing garlic extract as per our previous research work [28].

Fabrication of Ag/CNT nanocomposite modified SPE

Ag nanoparticles (NPs) were added to CNTs in different ratios. Based on prominent peak shape and highest current value, 1:3 ratios were optimized for Ag and CNTs, respectively. The nanocomposite was suspended in 1mL dimethylformamide (DMF) and was sonicated for 2hrs until homogenous suspension was observed in eppendorf. Before dropcoating the SPE electrode surface, the eppendorfs were vortexed thoroughly. Further, volume of 5 μ L of the nanocomposite was optimized for coating the SPE based on highest peak current values.

Characterization of the optimized modifier

XRD pattern

XRD patterns of Ag NPs, CNTs and Ag/CNT nanocomposite are presented in Figure.1. This was performed on the Bruker D8 advance X-ray diffractometer with CuK α radiation (1.5406 Å) for the phase composition of samples. The XRD pattern of Ag NPs, CNTs and Ag loaded CNTs are presented in Figure 1. The reflection planes (020), (111), (200) and (400) at corresponding 2theta angles are 30.8, 38.15, 44.19 and 51.6 which indicates the formation of face centered cubic (fcc) structure of Ag NPs. It was also matched with the standard pattern having JCPDS no. 4-0783 [29-33].

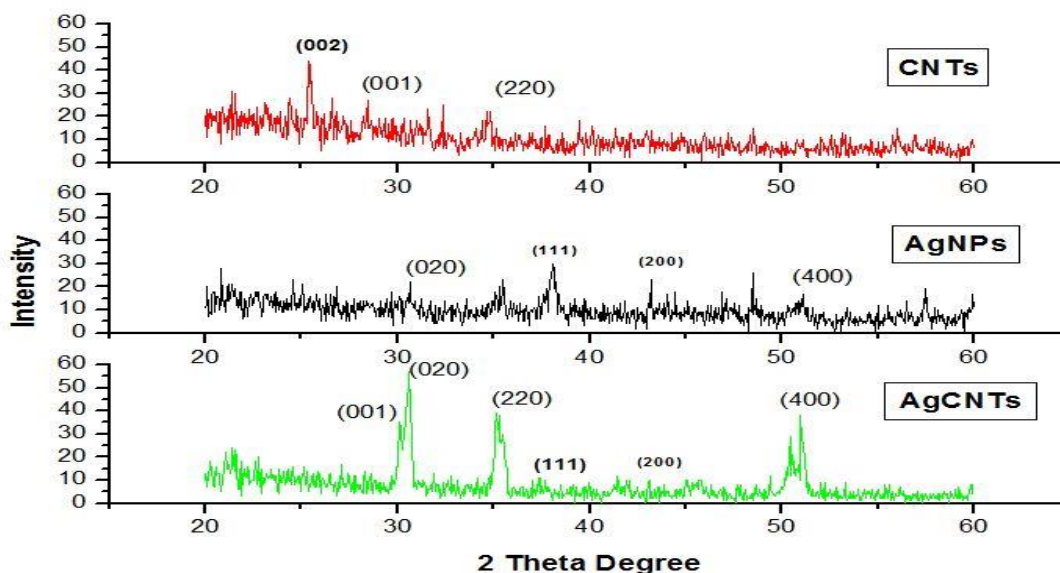


Figure 1. X-ray diffractogram of CNTs, Ag NPs and Ag/CNTs nanocomposite

FTIR analysis

The FTIR scale traced for concerned nanomaterial is displayed in Figure 2. For

Ag/CNT, nanocomposite considerable stretch positions are mentioned in the Table 1. with their respected wavelength range [34].

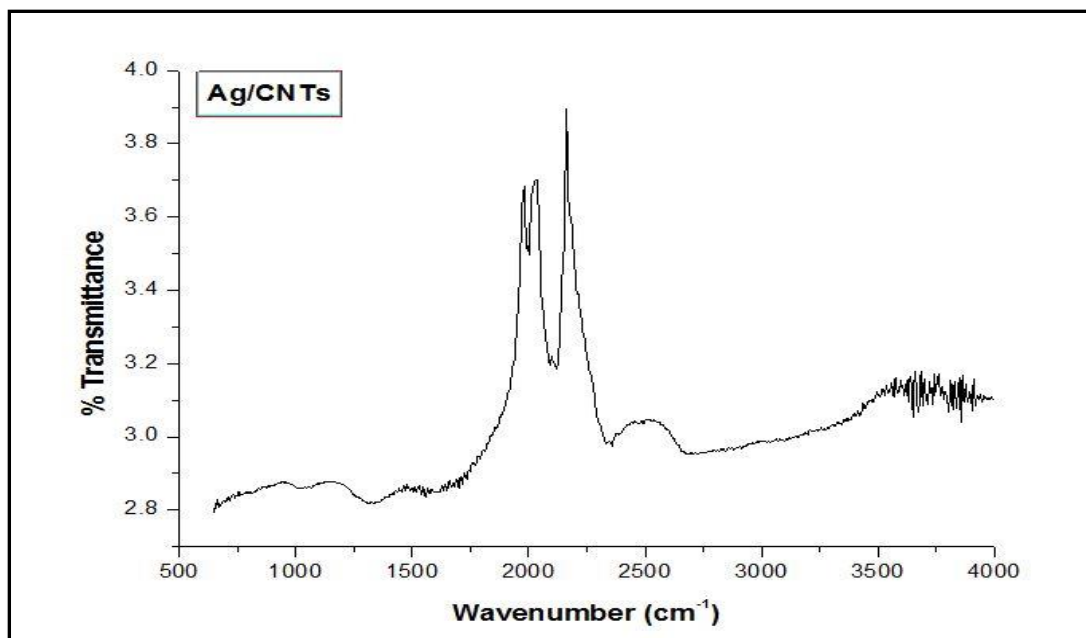


Figure 2. FTIR spectra of Ag/CNTs nanocomposite

Table 1. Detected peaks in Ag loaded functionalized CNTs FTIR

Wavelength range (cm ⁻¹)	Assignment
3500 - 3000	Bonded -OH group
2900 - 2800	CH stretching
2100 - 2150	-CN Stretching
1740 - 1680	C=O groups
1670 - 1640	Carboxylic group
1500 - 1430	Benzene ring Stretching
1600 - 1500	-NH bending
1400 - 1300	-NO ₂ Stretching
1280 - 1240	-SO ₃ ²⁻ stretching
1200 - 1000	-CO H stretch
910 - 650	Aromatic CH Bend

UV-Vis analysis

UV-Vis spectra were used to further verify the fabrication of Ag/CNT nanocomposite (Fig. 3). Aromatic C=C bonds containing π - π transitions are responsible for the absorption peak observed in the range of 250 - 300 nm (red curve). A characteristic broad peak at 360 - 600

nm range is seen in Ag/CNTs (black curve) spectrum which corresponds to surface plasmon absorption (SPR) of Ag nanoparticles. The appearance of peaks maxima at around 275 and 420 nm evidences the presence of CNTs and AgNPs. Excitation of SPR band is responsible for yellowish brown colour of Ag nanoparticles in aqueous solution [34, 35].

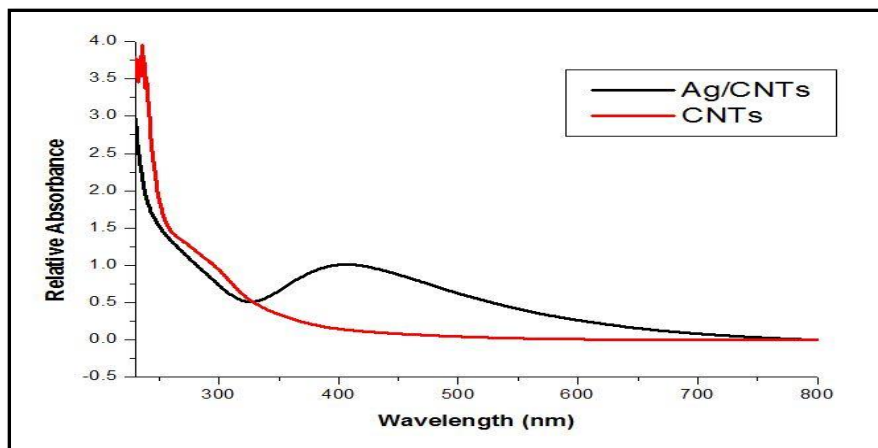


Figure 3. UV-Vis spectra of CNT and Ag/CNT nanocomposite

FESEM and EDX of the modifier

The surface structure and compositional analysis of Ag/CNT nanocomposite and its characteristic facets were scrutinized through FESEM and EDX techniques (Fig. 4). These large numbers of Ag NPs were effectively mixed with CNTs with minor agglomerates of NPs. The dimensions of Ag NPs were found to be less

than 20 nm and diameter for CNTs between 20 to 30 nm. The compositional analysis was affirmed via EDAX spectroscopy as depicted in (Fig. 4). It illustrates the occurrence of concerned element in the material which is studied with the preliminary material composition [36, 37]. By weight, percentage of Ag, O and C was found to be 0.19%, 3.06% and 96.75%, respectively.

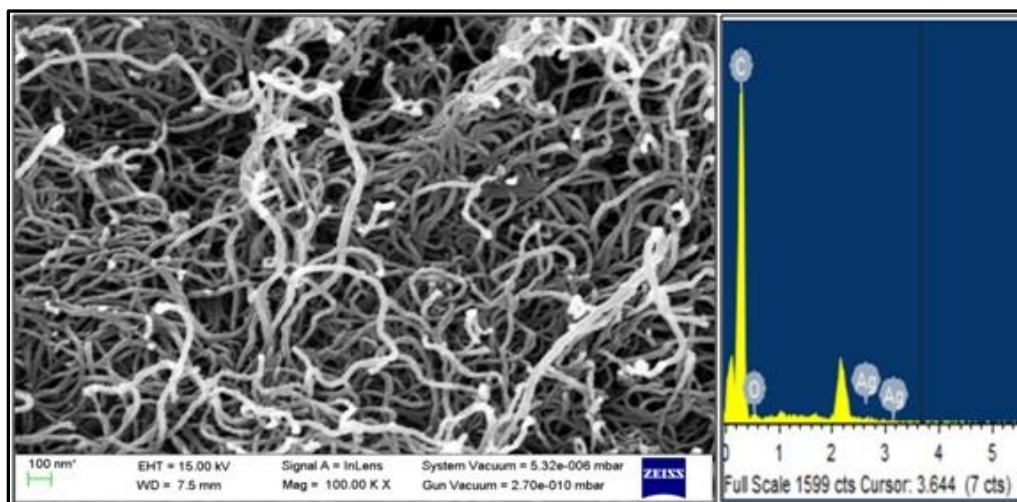


Figure 4. FESEM image and EDX spectra Ag/CNT nanocomposite

Results and Discussion

Electrochemical behaviour of BTR at Ag/CNT/SPE

Electrochemical investigation (CV and SWV) of BTR in B-R buffer at pH 4.5 was studied using fabricated sensors. Ag/CNT was prepared in three different ratios 1:2, 1:1 and 2:1, where 1:1

was optimized and used throughout the study owing to high peak current and stability. There is no anodic and cathodic peak with reference to Ag/CNT/SPE in blank buffer (Fig. 5); this indicates the nonreactive nature of modified material and also shows that it is electrochemically inactive with the selected potential window. There is modifier used for the modification of SPE in which Ag/CNTs/SPE

have maximum oxidation signal and on reverse scan there occurs no signal. This indicates the

irreversible behaviour of electro-oxidation reaction at the electrode interface.

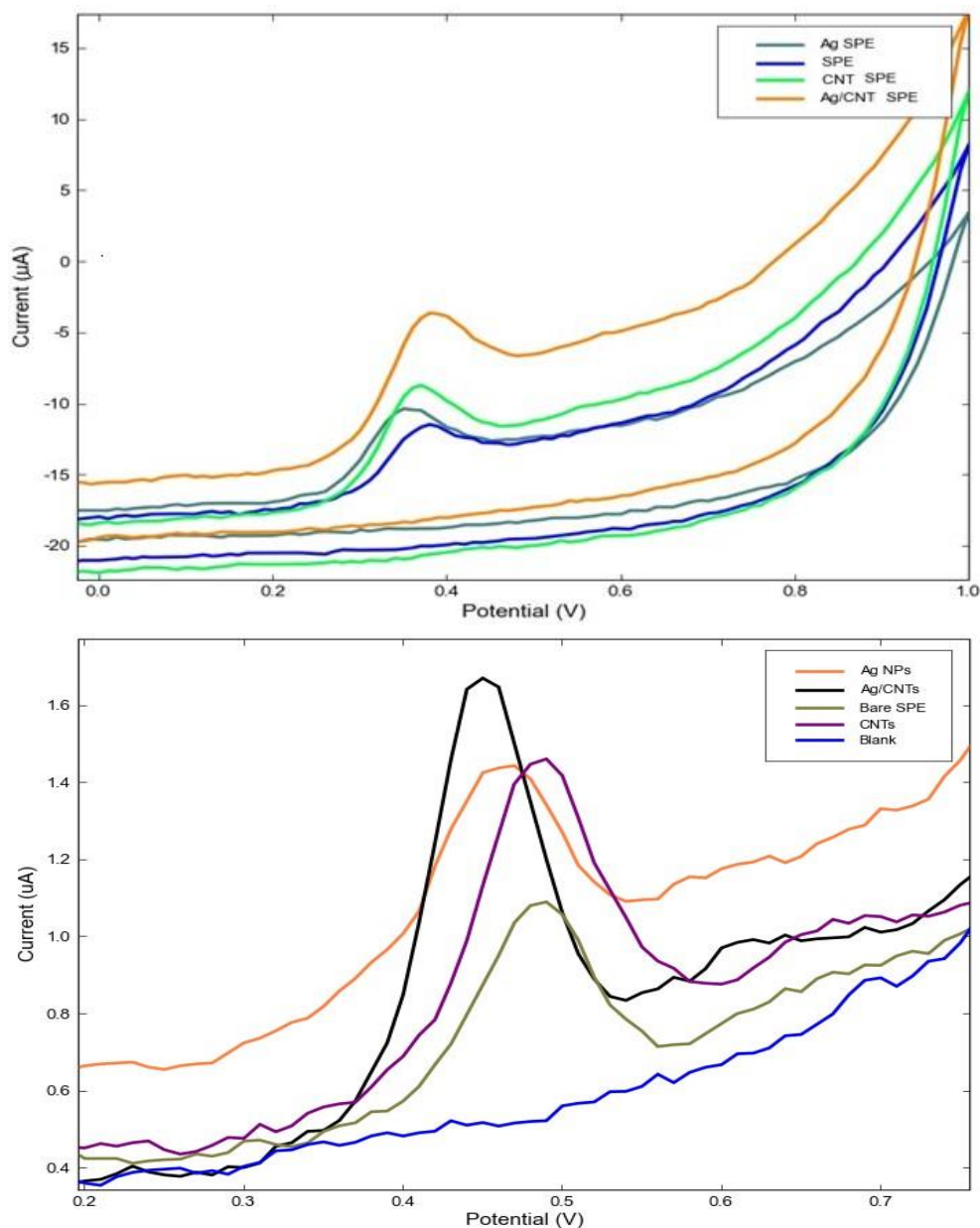


Figure 5. CV and SWV of BTR (4.5 pH) at bare and modified SPE

Figure 5. shows the CV and SWV of BTR at bare SPE, Ag/SPE, CNT/SPE, and Ag/CNT/SPE. A sharp peak was obtained for oxidation of BTR at Ag/CNT/SPE. The higher oxidation current suggests the enhanced charge transfer occurring at the modified electrode surface. The synergism between CNTs and AgNPs is the principle for the working modified electrode where superior electrical conductivity of the

sensor helps in quantification of analyte system in trace amounts.

Role of supporting electrolyte and its pH

The nature of supporting electrolyte and pH strongly influences the electrocatalytic behavior of the analyte system. In B-R buffer, electrodes gave excellent response among other buffers; therefore, the effect of pH on oxidation

behavior of BTR at Ag/CNT/SPE was studied using CV within pH range of 2.5 - 12.0. From the pH voltammograms (Fig. 6a) negative shift of peak with an increase in pH value has been observed which indicates protons involvement in the oxidation process at the electrode surface. Linearity E_p vs pH described the equation as $E_p = -0.0672 \text{ pH} + 0.8641$; $R^2 = 0.9701$. A negative slope of 0.0672 V/pH was

obtained. This value is closest to -0.059 V/pH which is the expected value of Nernst. These are the closest to each other so the same number of electrons and protons may be participating in the electro-oxidation of BTR [38]. It was also observed that pH 4.5 was optimized and chosen for further study based on peak shape and high current values.

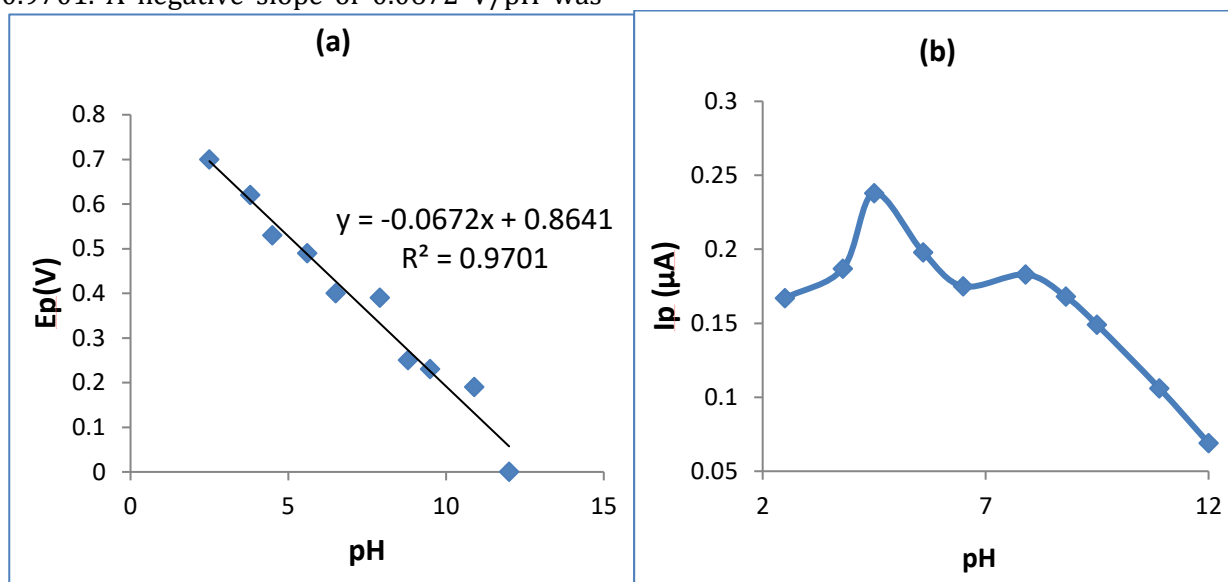
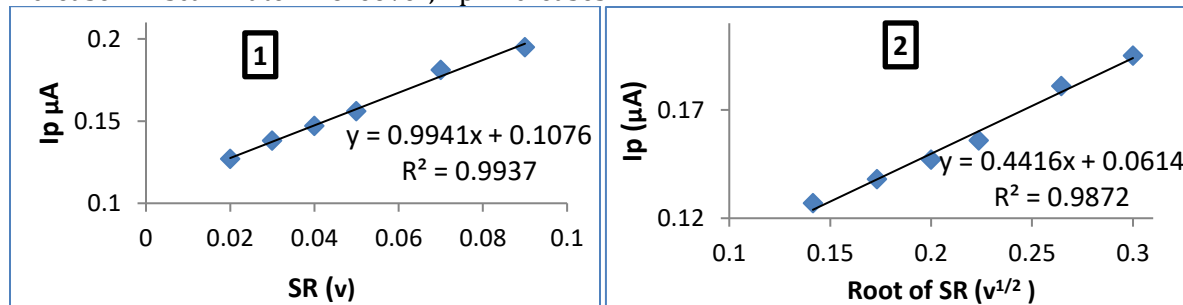


Figure 6. (a) pH vs E_p (V) curve and (b) pH vs I_p (μA) curve for BTR ($10.41 \mu\text{M}$) with Ag/CNTs/SPE

Effect of scan rate

For the investigation of scan rate (v) and kinetics of BTR at Ag/CNT/SPE, CV (Fig. 8) at varying v (20-90 mV/sec) was carried out under optimum conditions. Here, Figure. 7(1) shows the electro-oxidation peak current (I_p), which is observed getting increased with increase in scan rate. Moreover, I_p increases

linearly with $v^{1/2}$ as shown in Figure.7 (2). Figure.7(1 - 3) the equations I_p (μA) = $0.9941 v$ (mV/sec) + 0.1076 ; $R^2 = 0.9937$, I_p (μA) = $0.4416 v^{1/2}$ (mV/sec) + 0.0614 ; $R^2 = 0.9872$ and $\ln I_p$ (μA) = $2.7764 \ln v$ (mV/sec) - 2.4634 ; $R^2 = 0.9941$, confirms that the process of BTR oxidation at Ag/CNT/SPE is a diffusion-controlled phenomenon [39, 40].



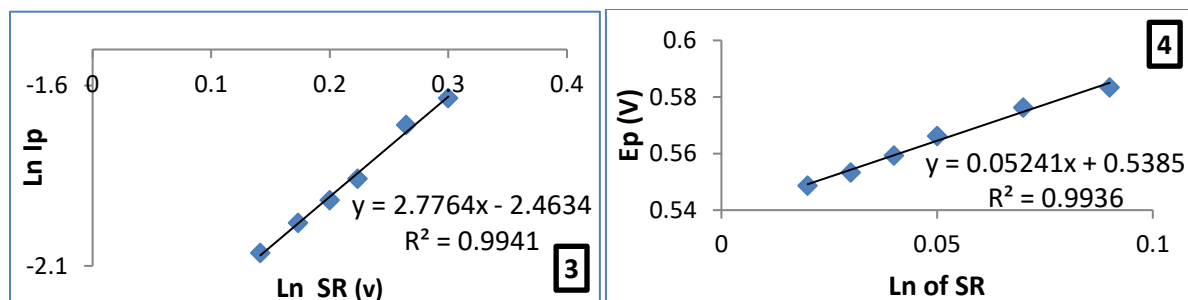


Figure 7. (1) scan rate vs I_p (μA), (2) $v^{1/2}$ vs I_p (μA) (3) Ln of Scan rate vs Ln of I_p (μA) (4) Ln of scan rate vs E_p (V)

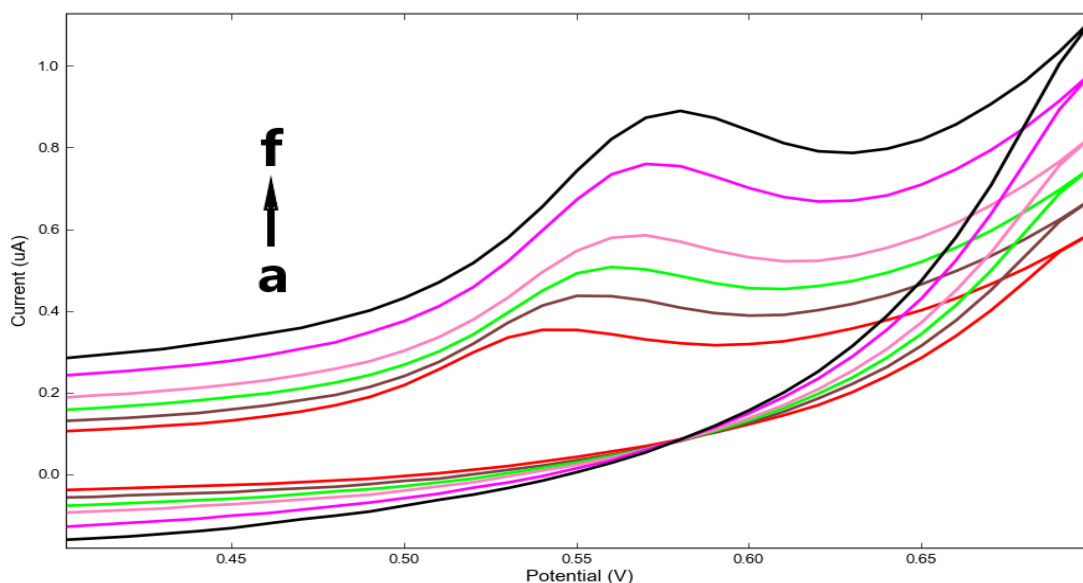


Figure 8. Cyclic voltammetric curves of BTR using Ag/CNT/SPE (pH 4.5 BR Buffer) at varying scan rates (20 to 90 mV/sec)

Relationship between E_p and v for an irreversible electrode process can be given as
 $E_p = E^0 + (RT/\alpha nF) \ln(RT k^0/\alpha nF) + (RT/\alpha nF) \ln v$

Here,

α = transfer coefficient,

k^0 = standard rate constant,

E^0 = formal potential,

n = number of electrons

v is the scan rate.

E_p vs $\ln v$ is shown in Figure. 7(4) and can be expressed as E_p (V) = 0.05241 $\ln v$ (mV/sec) + 0.05385; $R^2 = 0.9936$. Combining above equation we get:

$$RT/\alpha nF = 0.05241$$

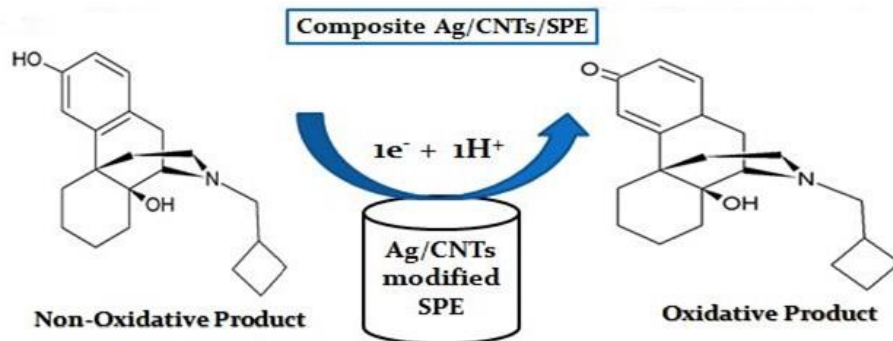
Where, $T = 298$ K, $R = 8.31$ J/K/mol and $F = 96500$ C. The value of αn can be calculated to be 0.49. For an irreversible redox process α is assumed to be 0.5. Thus, α is calculated to be 0.517. Based on all substitutions, electron transfer number (n) was calculated to be 1 [41, 42].

$$RT/\alpha nF = 0.05241$$

Further, the number of protons involved in the phenomenon was calculated using the equation as given below:

$$E_p = E^0 - 2.303 RT m [nF]^{-1} \log H^+$$

Where, E^0 indicate standard potential and 'm' is the number of protons which was found to be 1. Hence, the expected probable mechanism is explained as shown in Scheme 3.



Scheme 3. Possible mechanism of oxidation of BTR at Ag/CNT/SPE

Analytical performance

For the determination of the limit of detection and quantification and working range of fabricated electrode, Ag/CNT/SPE was utilized to study the electrocatalytic behavior of BTR within the selected potential range in SWV. Figure 9. shows the linearity between oxidation

peak current and concentration of BTR. Plots for BTR [Figure. 11] over a range of 1.05 to 10.42 μM can be shown as $I_p(\mu\text{A}) = 0.311\text{mg/l} + 0.1741$, $R^2 = 0.9999$. The LOD and LOQ was 2.15 μM and 7.18 μM calculated from $3S/B$ and $10S/B$, where S is the standard deviation and B is the slope of the calibration curve [42].

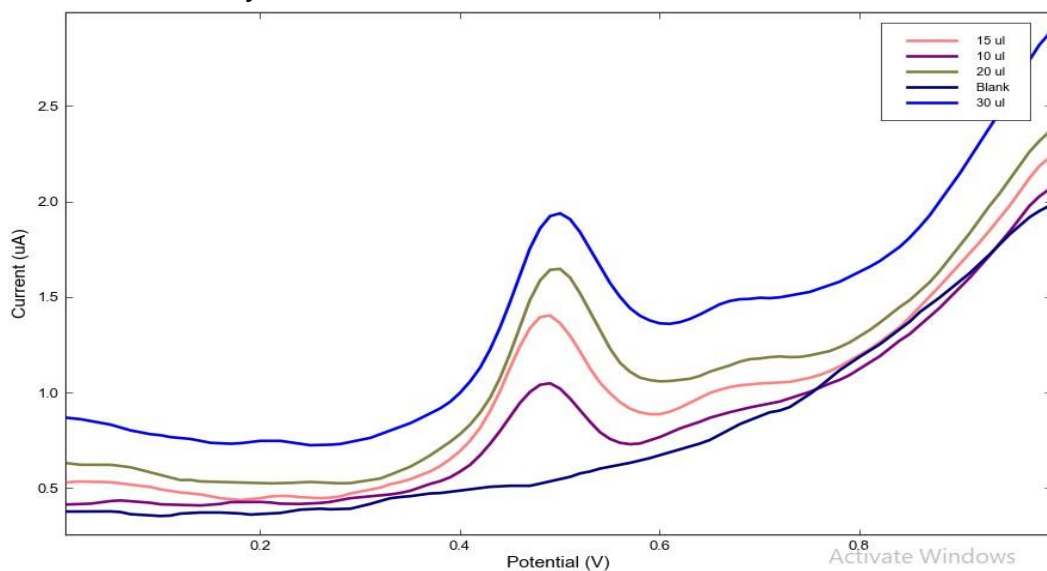


Figure 10. SWV of BTR (pH 4.5, 1.05 to 10.42 μM) using Ag/CNT/SPE electrode

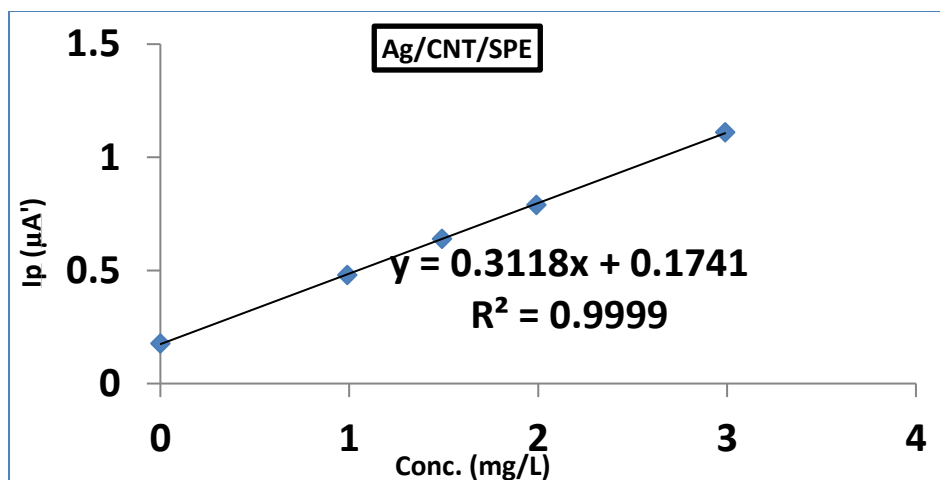


Figure 11. Calibration curve of I_p (μA) and concentration (mg/L) for Ag/CNT/SPE

Validation of the Method

Ag/CNT/SPE sensor was checked by taking 3 different SPE for validating results. A relative standard deviation (RSD) of 1.69% was found with acceptable reproducible values. Further, a scan of 6 replicate measurements using the same electrode gave an RSD of 1.3%. Thus,

Ag/CNT/SPE proved to be a promising tool for the study of redox analytes (Table 2).

The sensor was stored for 7 days at 4°C and after 7 days, the sensor was able to retain its performance more than 90% of its initial current values suggesting stability of Ag/CNT/SPE.

Table 2. Reproducibility and Repeatability results at Ag/CNTs/SPE

Sensor	Reproducibility		Repeatability	
	Mean I_p μA	% RSD	Mean I_p μA	% RSD
1	0.2393	2.29	0.2686	1.3
2	0.2208	1.01		
3	0.2809	1.04		
4	0.2579	1.82		
5	0.2168	2.31		
Avg	0.24314	1.694		

Accuracy and precision were found taking BTR in 3 varying concentrations (1, 3, and 5 μM). Here, RE represents the percentage

relative error, and precision is calculated using percentage relative standard deviation to find the coefficient of variance (Table 3).

Table 3. Accuracy and precision results for determination of BTR using SWV

St. Added (μM)	St. Found (μM)	Precision	COV%	RE %
1	0.961	0.96 ± 0.01	1.36	-3.93
3	2.974	2.97 ± 0.02	0.69	-0.86
5	5.022	5.02 ± 0.08	1.59	0.45

Recovery Analysis

BTR in Butrum injection (tablet labeled as 25 mg) was used directly from the market for

recovery studies. 3 replicate measurements were employed with 3 different concentrations (1, 3, and 5 μM). The recoveries were in the range 97.73–101.98% (Table 4).

Table 4. Recovery results of BTR in its pharmaceutical tablet

Added (μM)	Found (μM)	RSD %	% Recovery
1	0.98	2.37	97.73
3	3.02	1.94	100.81
5	5.09	1.87	101.98

Conclusion

A novel Ag/CNT nanocomposite-based screen-printed carbon sensor was fabricated for the quantification of BTR. The proposed analytical method offered high sensitivity with lower detection limits. The electrode dynamic processes revealed the mechanistic aspects of the electro-oxidation of BTR with one proton and one electron transfer taking place at the surface of the electrode. Scan rate and pH studies also showed the process to be a diffusion-controlled process. Good reproducibility and repeatability have been shown through the developed sensor. Thus, Ag/CNT/SPE can be used as a promising analytical tool for the study of pharmaceutical drugs.

Acknowledgments

The authors greatly acknowledge Dayalbagh Educational Institute, Agra for the research work and IIT Roorkee for characterization.

Funding

Financial assistance was provided by Dayalbagh Educational Institute, Agra.

Conflict of Interest

The authors declared that they do not have any conflict of interest regarding this research article.

Orcid:

Manish S Sengar :

<https://orcid.org/0000-0002-5410-9904>

Sachin Saxena :

<https://orcid.org/0000-0001-9700-6676>

Soami P. Satsange :

<https://orcid.org/0000-0002-4605-0535>

Rajeev Jain :

<https://orcid.org/0000-0001-5418-6400>

References

- [1] J. Lenik, *Curr. Med. Chem.*, **2017**, *24*, 2359-2391. [[Crossref](#)], [[Google scholar](#)], [[Publisher](#)]
- [2] F. Arduini, L. Micheli, D. Moscone, G. Palleschi, S. Piermarini, F. Ricci, G. Volpe, *Trends Analyt. Chem.*, **2016**, *79*, 114-126, [[crossref](#)], [[Google scholar](#)], [[Publisher](#)]
- [3] P. Chuntib, S. Themsirimongkon, S. Saipanya, J. Jakmune, *Talanta*, **2017**, *170*, 1-8, [[crossref](#)], [[Google scholar](#)], [[Publisher](#)].
- [4] F. Lopes, J. G. Pacheco, P. Rebelo, C.D. Matos, *Sens. Actuat. B Chem.*, **2017**, *243*, 745-752, [[Crossref](#)], [[Google scholar](#)], [[Publisher](#)]
- [5] R. Gusmão, V. L. Puente, L. Yate, I.P. Santos, J.P. Juste, E.G. Romero, *Mater. Today Commun.*, **2017**, *11*, 11-17, [[crossref](#)], [[Google scholar](#)], [[Publisher](#)]
- [6] J. Agrisuelas, M.I.G. Sánchez, E. Valero, *Sens. Actuat. B Chem.*, **2017**, *249*, 499-505, [[Crossref](#)], [[Google scholar](#)], [[Publisher](#)].
- [7] Q. Qin, X. Bai, Z. Hua, *J. Electroanal. Chem.*, **2016**, *782*, 50-58, [[crossref](#)], [[Google scholar](#)], [[Publisher](#)]
- [8] N.H. Ibáñez, L.G. Cruz, V. Montiel, C.W. Foster, C.E. Banks, J. Iniesta, *Biosens. Bioelectron.*, **2016**, *77*, 1168-1174, [[crossref](#)], [[Google scholar](#)], [[Publisher](#)].
- [9] L. M. Ochiai, D. Agustini, L. C. S. F. Filho, C.E. Banks, L. H. M. Junior, M.F. Bergamini, *Sens. Actuat. B Chem.*, **2017**, *241*, 978-984, [[crossref](#)], [[Google scholar](#)], [[Publisher](#)]
- [10] P. Bollella, G. Fusco, C. Tortolini, G. Sanzò, G. Favero, L. Gorton, R. Antiochia, *Biosens. Bioelectron.*, **2017**, *89*, 152-166, [[Crossref](#)], [[Google scholar](#)], [[Publisher](#)]
- [11] G. I. N. Redín, D. Wilson, D. Gonçalves, O.N. Oliveira, *J. Colloid Interface Sci.*, **2017**, *515*, 101-108, [[Crossref](#)], [[Google Scholar](#)], [[Publisher](#)].

- [12] S. Ansari, M.S. Ansari, S.P. Satsangee, R. Jain, *Anal. Chim. Acta.*, **2019**, *1046*, 99-109, [[Crossref](#)], [[Google scholar](#)], [[Publisher](#)]
- [13] S. Ansari, M.S. Ansari, H. Devnani, S.P. Satsangee, R. Jain, *Sensor Actuat B: Chem.*, **2018**, *273*, 1226-1236, [[Crossref](#)], [[Google scholar](#)], [[Publisher](#)]
- [14] S. Lim, Z.R. Melrose, E.T. Thostenson, T.W. Chou, *Compos. Sci. Technol.*, **2011**, *71*, 1183-1189, [[Crossref](#)], [[Google scholar](#)], [[Publisher](#)]
- [15] R.Y.A. Hassan, M.A. Sultan, M.M. A.E. Alamin, M.A. Atia, H.Y.A. Enein, *Electroanal.*, **2017**, *29*, 843 - 849, [[crossref](#)], [[Google scholar](#)], [[Publisher](#)]
- [16] Q. Zhao, S. Tan, M. Xie, Y. Liu, J. Yi, *J. Alloy. Compd.*, **2018**, *737*, 31-38, [[Crossref](#)], [[Google scholar](#)], [[Publisher](#)]
- [17] X. Yan, S. Li, J. Bao, N. Zhang, B. Fan, R. Li, X. Liu, Y. X. Pan, *ACS Appl. Mater. Interfaces.*, **2016**, *8*, 17060-17067, [[crossref](#)], [[Google scholar](#)], [[Publisher](#)]
- [18] D.W. Boulton, G. F. Duncan, N. N. Vachharajani, *J. Chromatogr. B.*, **2002**, *775*, 57-62, [[crossref](#)], [[Google scholar](#)], [[Publisher](#)]
- [19] M. D. Smith, B. A. Connor, H. I. Karunadasa, *Chem. Rev.*, **2019**, *119*, 3104-3139, [[crossref](#)], [[Google scholar](#)], [[Publisher](#)]
- [20] G. Landberg, E. Jonasson, A. Gustafsson, P. Fitzpatrick, P. Isakson, J. Karlsson, E. Larsson, A. Svanström, S. Rafnsdóttir, E. Persson, D. Andersson, J. Rosendahl, S. Petronis, P. Ranji, P. Gregersson, Y. Magnusson, J. Hakansson, A. Stahlberg, *Data Brief. (Biomaterials)*, **2020**, *235*, 119705, [[Crossref](#)], [[Google scholar](#)], [[Publisher](#)]
- [21] J. Piechocka, M. Wronska, G. Chwatko, H. Jakubowski, R. Glowacki, *J. Chromatogr. B.*, **2020**, *1149*, 122155, [[crossref](#)], [[Google scholar](#)], [[Publisher](#)]
- [22] Z. Mala, P. Gebauer, *Electrophor.*, **2018**, *0*, 1-10, [[Crossref](#)], [[Google scholar](#)], [[Publisher](#)]
- [23] S. Boonkaew, P. Teengam, S. Jampasa, S. Rengpipat, W. Siangproh, O. Chailapakul, *Analyst.*, **2020**, *14*, 1-8, [[Crossref](#)], [[Google scholar](#)], [[Publisher](#)]
- [24] M. Niwa, T. Nose, M. Nozaki, K. Tsurumi, H. Fujimura, *Japan. J. Pharmacol.*, **1985**, *39*, 515-528, [[Crossref](#)], [[Google scholar](#)], [[Publisher](#)]
- [25] E. Troncy, J. G. Besner, R. Charbonneau, S. G. Cuvelliez, D. Blais, *J. Vet. Pharmacol. Therap.*, **1996**, *19*, 268-273, [[crossref](#)], [[Google scholar](#)], [[Publisher](#)]
- [26] M. S. Sengar, S. Saxena, A. Lakhani, S. P. Satsangee, *Asian J. Green Chem.*, **2021**, *5*, 206-218, [[Crossref](#)], [[Google scholar](#)], [[Publisher](#)]
- [27] G. J. H. Melvin, Q. Q. Ni, T. Natsuki, Z. Wang, S. Morimoto, M. Fujishige, K. Takeuchi, Y. Hashimoto, M. Endo, *Synth. Met.*, **2015**, *209*, 383-388, [[crossref](#)], [[Google Scholar](#)], [[Publisher](#)]
- [28] D. A. Skoog, D. M. West, F. J. Holler, S. R. Crouch, *Fundamentals of Analytical Chemistry*, Mary Flinch, Belmont, CA, USA, **2013**; p 1072.
- [29] F. Wu, D. Liu, T. Wang, W. Li, X. Zhou, *J. Mater. Sci.: Mater. Electron.*, **2015**, *26*, 6781-6786, [[crossref](#)], [[Google scholar](#)], [[Publisher](#)]
- [30] V. Mani, M. Govindasamy, S.M. Chen, T. W. Chen, A. S. Kumar, S. T. Huang, *Sci. Rep.*, **2017**, *7*, 11910, [[Crossref](#)], [[Google scholar](#)], [[Publisher](#)]
- [31] Q. Zhang, L. Liu, D. Zhao, Q. Duan, J. Ji, A. Jian, W. Zhang, S. Sang, *Nanomater.*, **2017**, *7*, 1-12, [[Crossref](#)], [[Google scholar](#)], [[Publisher](#)]
- [32] R. X. Dong, C. T. Liu, K. C. Huang, W. Y. Chiu, K. C. Ho, J. J. Lin, *ACS Appl. Mater. Interfaces.*, **2012**, *4*, 1449-1455, [[Crossref](#)], [[Google scholar](#)], [[Publisher](#)]
- [33] F. Tian, X. Dong, Z. Zhao, J. He, H. T. Wang, *J. Phys.: Condens. Matter.*, **2012**, *24*, 165504, [[Crossref](#)], [[Google Scholar](#)], [[Publisher](#)]
- [34] G. H. Priyaa, K. B. Satyan, *J. Environ. Nanotechnol.*, **2014**, *3*, 32-40, [[Crossref](#)], [[Google scholar](#)], [[Publisher](#)]
- [35] Y. Dou, H. Liu, J. Peng, M. Li, W. Li, F. Yang, *J. Mater. Sci.*, **2016**, *51*, 5685-5694, [[Crossref](#)], [[Google scholar](#)], [[Publisher](#)]
- [36] M. Satyanarayana, K. Y. Goud, K. K. Reddy, V. S. Kumar, K. V. Gobi, *Mater. Sci. Eng. C.*, **2019**, *101*, 103-110, [[Crossref](#)], [[Google scholar](#)], [[Publisher](#)]
- [37] S. H. Lee, C. C. Teng, C. C. M. Ma, I. Wang, *J. Colloid Interface Sci.*, **2011**, *364*, 1-9, [[Crossref](#)], [[Google scholar](#)], [[Publisher](#)]

- [38] L. Li, L. R. Xia, H. Y. Wang, X. D. Bi, *J. Appl. Polym. Sci.*, **2015**, *132*, 41792, [[crossref](#)], [[Google scholar](#)], [[Publisher](#)]
- [39] N. Elgrishi, K. J. Rountree, B. D. McCarthy, E. S. Rountree, T. T. Eisenhart, J. L. Dempsey, *ACS J. Chem. Edu.*, **2018**, *95*, 197-206, [[crossref](#)], [[Google scholar](#)], [[Publisher](#)]
- [40] J. MacLeod, *Appl. Math. Comput.*, **1993**, *57*, 305-310, [[Crossref](#)], [[Google Scholar](#)], [[Publisher](#)]
- [41] M. L. Yola, V. K. Gupta, T. Eren, A. E. Şen, N. Atar, *Electrochim. Acta.*, **2014**, *120*, 204-211, [[Crossref](#)], [[Google scholar](#)], [[Publisher](#)].
- [42] M. L. Yola, N. Atar, T. Eren, H. K. Maleh, S. Wang, *RSC Adv.*, **2015**, *5*, 65953-65962, [[crossref](#)], [[Google Scholar](#)], [[Publisher](#)]

Copyright © 2021 by SPC ([Sami Publishing Company](#)) + is an open access article distributed under the Creative Commons Attribution License (CC BY) license (<https://creativecommons.org/licenses/by/4.0/>), which permits unrestricted use, distribution, and reproduction in any medium, provided the original work is properly cited.